Molecular Catalysis 587 (2025) 115473

Contents lists available at ScienceDirect

Molecular Catalysis

journal homepage: www.journals.elsevier.com/molecular-catalysis

Research Paper

2D Materials unleashed: Pyrrole-nitrobenzylidene copolymers for advanced photocatalysis for water-splitting technologies

Abderrahmane Remil [a], Mohamed El Amine El Goutni [b], Talal M. Althagafi [c], Mokhtar Saidi [a], Hamza Belkhodja [d], Abdelkrim Bendoukha Reguig [a], Mohammed El Amine Monir [e], M. Fatmi [f,*], M.A. Ghebouli [f,g]

[a] Laboratory of Organic, Macromolecular chemistry and Materials, University of Mustapha Stambouli, Mascara, Algeria
[b] Laboratory of Quantum Physics of Matter and Mathematical Modeling, University of Mustapha Stambouli, Mascara, Algeria
[c] Department of Physics, College of Sciences, Taif University, P.O. Box 11099, Taif 21944, Saudi Arabia
[d] Laboratory of Bioconversion, Microbiology Engineering and Health Safety, University of Mustapha Stambouli, Mascara, 29000, Algeria
[e] Faculty of the Exact Sciences, Mustapha Stambouli, University of Mascara, B.P. 305, Mascara 29000, Algeria
[f] Research Unit on Emerging Materials (RUEM), University Ferhat Abbas of Setif 1, Setif, 19000, Algeria
[g] Department of Chemistry, Faculty of Sciences, University of M'sila, University Pole, Road Bourdj Bou Arreiridj, 28000, M'sila, Algeria

ARTICLE INFO

Keywords:
Conjugated copolymers
Thin films
Photocatalysis
Water splitting
Hydrogen evolution
Co_2 reductions

ABSTRACT

The objective of this work is to explore the optical, morphological, and photocatalytic properties of two innovative conjugated copolymers: poly(2,5-diyl pyrrole) [3-nitrobenzylidene] (PP3NB) and poly(2,5-diyl pyrrole) [2,4-dinitrobenzylidene] (PPDNB). These copolymers were synthesized by condensation, and their thin films were prepared by dip-coating. This is followed by characterization by UV–Vis spectroscopy, scanning electron microscopy (SEM), and cyclic voltammetry (CV). Optical analysis revealed a broad absorption in the visible spectrum, with band gaps of approximately 2.1 eV for PP3NB and 1.98 eV for PPDNB. Morphological characterization revealed the formation of uniform and adherent films to the substrate, with tunable surface roughness, which influences the charge transport characteristics. Electrochemical calculations established the HOMO–LUMO energy levels, showing good alignment with typical donor–acceptor systems. The effective masses of charge carriers, derived from the HOMO–LUMO band gaps and conjugation lengths, were 0.00635 m_e for PP3NB and 0.00596 m_e for PPDNB, indicating improved charge mobility. Based on the band edge positions, the photocatalytic potential evaluation suggests that PPDNB demonstrates superior capabilities for reduction reactions, especially in hydrogen evolution and CO_2 reduction, while PP3NB excels in oxidation processes. These results highlight the versatility and efficiency of pyrrole-nitrobenzylidene copolymers for renewable energy conversion and environmental remediation applications, highlighting their potential in organic solar cells, photocatalysis, and water-splitting technologies.

1. Introduction

The transformative influence of low-dimensional materials on nanoscale material properties is well-established [1]. Among these, thin films classified as two-dimensional (2D) materials with thicknesses ranging from nanometers to micrometers have driven significant technological progress in healthcare, energy, and environmental applications [2,3]. Their unique structure enables quantum confinement of electrons in one dimension while allowing unrestricted movement in the other two, blending bulk and nanoscale properties. This synergy and structural flexibility make thin films highly valuable for applications such as electronic displays, smart windows, and sensors. Unlike bulk materials, thin films feature atomically ordered structures that integrate seamlessly into devices with inherent functionalities [4]. Thin films offer a robust approach to material structuring, facilitating device miniaturization. The confinement of electric charges within their limited dimensions heightens interfacial sensitivity, profoundly affecting material properties [5]. Recent progress in material structure physics has introduced new challenges in synthesis, characterization, and modeling, particularly for application-specific designs. In thin films, size and

* Corresponding author.
E-mail addresses: t.althagafi@tu.edu.sa (T.M. Althagafi), fatmimessaoud@yahoo.fr (M. Fatmi).

https://doi.org/10.1016/j.mcat.2025.115473

Available online 10 September 2025

morphology play a decisive role in tuning properties to meet targeted feasibility criteria. In the current drive for tunable materials and adaptable fabrication methods for energy and environmental solutions, photocatalysis stands out as a versatile and scalable approach [6]. By harnessing light-driven redox reactions to generate reactive species, photocatalysis enables applications such as water splitting for hydrogen and oxygen production, pollutant degradation, CO_2 conversion to hydrocarbon fuels, and microbial disinfection. Its broad applicability makes it a strong candidate for large-scale deployment. However, achieving high photocatalytic efficiency demands careful photocatalyst design, incorporating (i) an optimal bandgap, (ii) suitably positioned band edges, (iii) minimized charge recombination, (iv) enhanced charge separation, and (v) efficient charge transport [7]. These characteristics can be attained through chemical modifications including doping, composite formation, metal sensitization, and molecular functionalization as well as physical strategies such as controlling size, shape, and surface morphology. Thin films, produced via bottom-up deposition of materials in the molecular phase onto substrates, represent a key structural innovation. They can remain substrate-bound or be detached for standalone use, offering benefits such as ease of handling, compatibility with reactor configurations, recyclability, and straightforward recovery, supporting the scaling of photocatalytic applications and underscoring the importance of their strategic design [8].

Building on our prior research into organic photovoltaic cells [9], this study investigates the photocatalytic potential of two novel conjugated copolymers: poly(2,5-diyl pyrrole) [3-nitrobenzylidene] (PP3NB) and poly(2,5-diyl pyrrole) [2,4-dinitrobenzylidene] (PPDNB). Synthesized via condensation reactions, these copolymers incorporate pyrrole and nitrobenzylidene derivatives to assess the impact of substituents on optoelectronic and photocatalytic feasibility. Thin films were fabricated using a cost-effective dip-coating method with dichloromethane solutions and characterized through UV–Vis spectroscopy, scanning electron microscopy (SEM), and cyclic voltammetry. The results reveal broad visible-light absorption (optical bandgap ~2 eV), uniform film morphologies with tunable roughness, and HOMO-LUMO energy levels well-aligned with common donor/acceptor materials. These attributes position the copolymers as promising candidates for multi-junction organic solar cells and photocatalysts, where optimized band structures and interfacial properties enhance charge separation and redox activity. This dual functionality highlights the versatility of substituent-modified pyrrole-nitrobenzylidene copolymers in advancing energy conversion and catalytic technologies.

2. Photocatalytic process: underlying mechanisms

In the photocatalytic process, light energy excites electrons in a semiconductor photocatalyst from the valence band (VB) to the conduction band (CB), generating electron-hole pairs. The excited electrons in the CB drive reduction reactions, while the holes in the VB promote oxidation reactions [10]. Interaction of these charge carriers with water molecules produces superoxide anions (O_2^-) and hydroxyl radicals (•OH) via redox reactions. These reactive species subsequently enable key transformations such as pollutant degradation, water splitting for hydrogen and oxygen production, and CO_2 reduction to methane defining the photocatalytic mechanism, as depicted in Fig. 1(a). The process thus supports diverse applications, including environmental remediation and energy conversion.

$$Sc + h\nu \rightarrow e^- + h^+ \quad (1)$$

$$e^- + O_2 \rightarrow O_2^{\bullet} \quad (2)$$

$$4e^- + 4H^+ \rightarrow 2H_2 \quad (3)$$

$$4h^+ + 2H_2O \rightarrow O_2 + 4H^+ \quad (4)$$

$$CO_2 + 2H + 2e^- \rightarrow HCOOH \quad (5)$$

A critical factor in designing photocatalytic materials as thin films is modifying their band structure to optimize the energy requirements of redox reactions. This is accomplished by aligning the band edge potentials within the thin film photocatalyst to promote efficient charge transfer [11]. For example, Fig. 1(b) depicts various conduction band (CB) and valence band (VB) edge positions that enable redox processes. It illustrates that complete water splitting requires a CB potential that is more negative and a VB potential that is more positive than that of the standard hydrogen electrode (NHE) scale [12].

3. Experimental details

3.1. Materials

Pyrrole and two benzaldehyde derivatives, 3-nitrobenzaldehyde and 2,4-dinitrobenzylidene, were purchased from Sigma Aldrich. The monomers and solvents were distilled under reduced pressure to ensure high purity. Dichloromethane (CH_2Cl_2) was used as received without further purification.

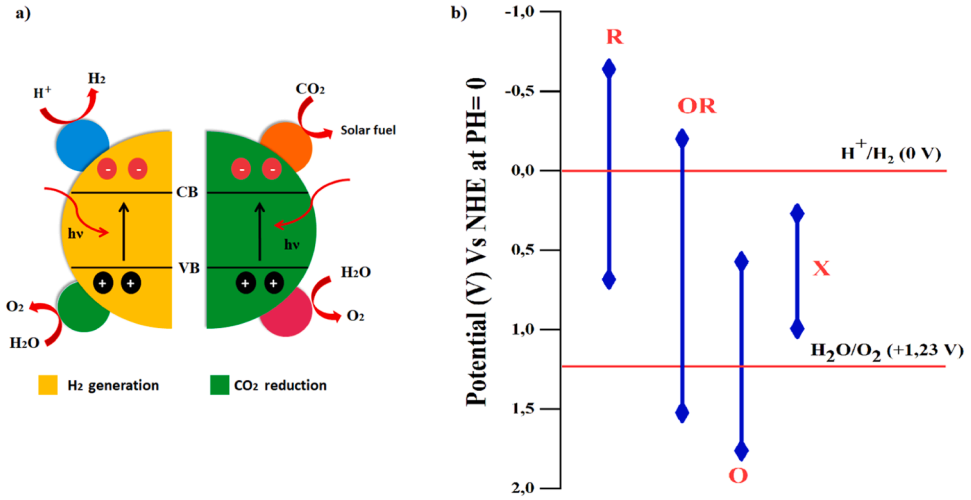

Fig. 1. (a) Photocatalytic process in semiconductor, (b) band edge potential and respective redox reactions (R: Reduction, O: Oxidation, OR: Oxidation & Reduction, X: no reaction).

3.2. Copolymers synthesis

The copolymers were synthesized via a condensation reaction between benzaldehyde derivative monomers and pyrrole, as outlined in Fig. 2, using Mag-H⁺ as a catalyst. The reaction occurred in a solution under a nitrogen atmosphere for 6 h. For each copolymer, 10 mmol of a specific benzaldehyde derivative and 10 mmol of pyrrole were dissolved in 15 mL of 1,2-dichloromethane. The Mag-H⁺ catalyst was dried at 100 °C for 1 hour, and 10 % of the weight of the dried catalyst was added to the mixture. The reaction was maintained at 25 °C for 6 h. Upon completion, the mixture was filtered to remove the clay catalyst, and the resulting polymer was precipitated by gradually adding methanol with stirring. The precipitated copolymer was collected and dried at room temperature under a controlled atmosphere for 24 h, yielding two distinct copolymers.

1. Poly (2,5-diyl pyrrole) [3-nitrobenzylidene] (PP3NB)
2. Poly (2,5-diyl pyrrole) [2,4-dinitrobenzylidene] (PPDNB),

The synthesized copolymers were characterized using nuclear magnetic resonance (NMR) spectroscopy and matrix-assisted laser desorption/ionization time-of-flight (MALDI-TOF) mass spectrometry to confirm their molecular structures and weights.

3.3. Fabrication of dip-coated copolymer thin films

Thin films of the synthesized copolymers were prepared via a dip-coating technique. The copolymers were dissolved in dichloromethane (CH_2Cl_2) to form homogeneous solutions for deposition. Glass substrates were thoroughly cleaned and dried before coating to ensure strong film adhesion. An automatic dip-coater, which controls immersion and withdrawal speeds, was used, with substrates coated back-to-back in pairs to prevent backside deposition. The process involved 25 cycles at a withdrawal speed of 0.5 mm/s, with ultrasonic stirring applied between immersions to maintain solution uniformity and avoid aggregation. Post-deposition, the coated substrates were annealed at 80 °C for 1 hour in an inert atmosphere to remove residual solvent, yielding uniform, continuous thin films with thicknesses of 35–38 nm, as verified by cross-sectional scanning electron microscopy (SEM). Surface morphology varied with copolymer composition, ranging from smooth to granular or rough textures, potentially affecting optoelectronic and photocatalytic properties. The films were subsequently analyzed for their optical, morphological, and electrochemical characteristics. The synthesized copolymers and their dip-coated thin films were characterized using various techniques to evaluate their optical, morphological, and electrochemical properties. Optical properties were assessed using a Perkin-Elmer Lambda 950 UV–Vis-NIR spectrophotometer with an integrating sphere. The thin films' absorption spectra were measured in the visible range at room temperature, with a scan rate of 60 nm/min. The optical bandgap (Eg) was determined from these spectra via Tauc plots, offering insights into the copolymers' light-harvesting potential.

The dip-coated thin films' surface topography and cross-sectional morphology were analyzed using a JEOL F-7600 field emission scanning electron microscope (SEM). High-resolution images captured in backscattered mode enabled detailed film uniformity, thickness, and surface roughness evaluation. SEM analysis confirmed film continuity and highlighted morphology variations linked to copolymer composition. The electrochemical properties of the copolymers were evaluated via cyclic voltammetry (CV) using a PGZ 301-Voltalab 10 potentiostat/galvanostat (Radiometer). Measurements were conducted in a 0.1 M tetrabutylammonium perruthenate (TBAP) electrolyte solution under a nitrogen atmosphere at room temperature, with a scan rate of 100 mV/s. Oxidation (Ep) and reduction (En) potentials were determined and used to calculate the highest occupied molecular orbital (HOMO) and lowest

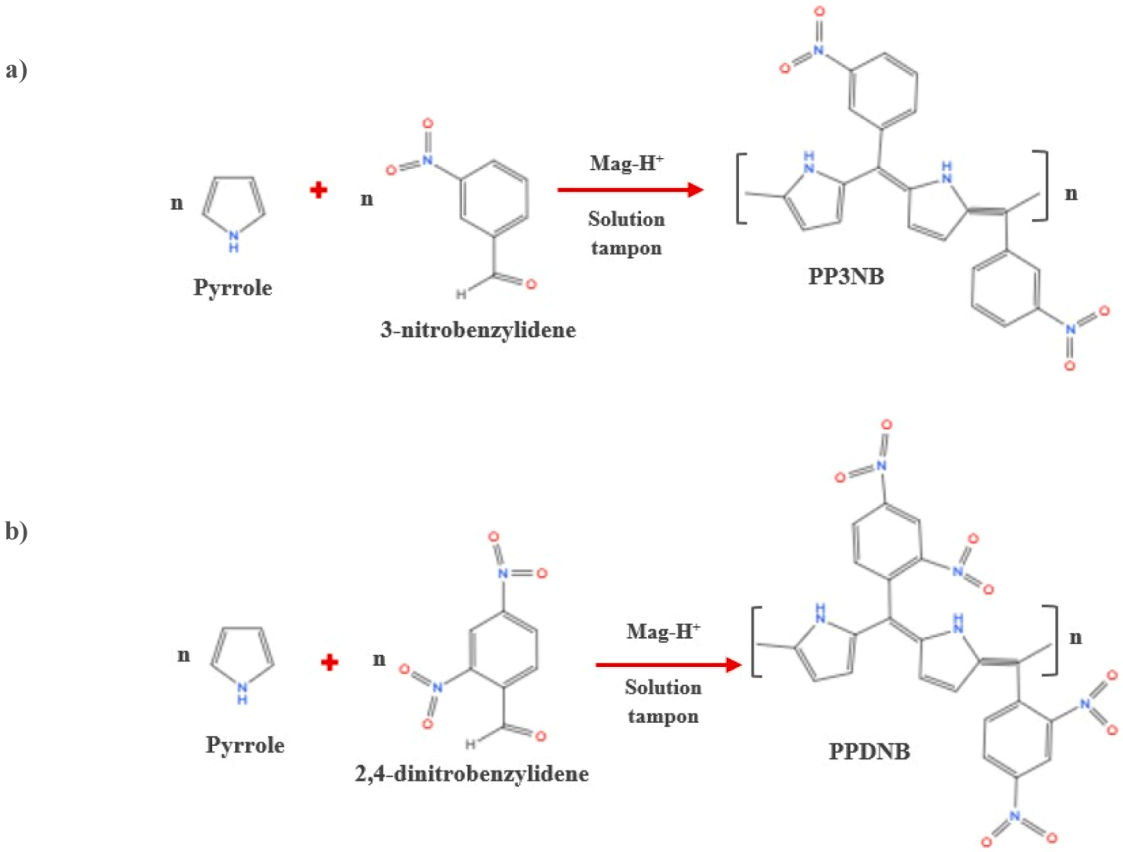

Fig. 2. Standard procedure for preparing P: P–B dip-coated thin film surfaces with various benzylidene derivatives: (a) PP3NB, (b) PPDNB.

unoccupied molecular orbital (LUMO) energy levels based on established equations.

$$E_{HOMO} = -(E_p + 4.4eV) \quad (6)$$

$$E_{LUMO} = -(E_n + 4.4eV) \quad (7)$$

The energy gap (*Eg*) was calculated as the difference between the LUMO and HOMO levels.

The synthesized copolymers' molecular weights were measured using matrix-assisted laser desorption/ionization time-of-flight (MALDI-TOF) mass spectrometry. This method verified the polymer structures and yielded precise molecular weight values consistent with the anticipated copolymer compositions. Together, these characterization techniques offered a thorough assessment of the copolymers' optical, morphological, and electrochemical properties, facilitating their evaluation for applications in organic solar cells and photocatalytic systems.

4. Results and discussion

4.1. Copolymer's analysis

The synthesized copolymers were characterized using nuclear magnetic resonance (NMR) spectroscopy and matrix-assisted laser desorption/ionization time-of-flight (MALDI-TOF) mass spectrometry to confirm their molecular structures and weights. The results are summarized below:

The $\mathbf{H^1}$ NMR spectrum of poly(2,5-dial pyrrole) [3-nitrobenzylidene] (PP3NB) $CDCl_3$, 300 MHz) exhibits characteristic signals corresponding to pyrrole protons at δ = 7.792 and 7.819 ppm (each appearing as a doublet, 1H each). The NH proton of the pyrrole ring is observed as a singlet at δ = 10.137 ppm. The aromatic protons of the 3-nitrobenzene moiety resonate at δ = 8.24, 8.268, 8.492, and 8.726 ppm (doublets, 1H each). The $\mathbf{C^{13}}$ NMR spectrum displays pyrrole carbon signals at 128.634 ppm (*C* = *C*) and 130.442 ppm (C—N). The 3-nitrobenzylidene moiety presents peaks at 134.740, 137.363, and 148.747 ppm (*C* = *C*), with the imine carbon observed at 189.852 ppm (C—N). Additional peaks at 124.476 ppm correspond to a (*C* = *C*—C).

For poly (2,5-dial pyrrole) [2,4-dinitrobenzylidene] (PPDNB), the H^1 NMR spectrum ($CDCl_3$, 300 MHz) reveals pyrrole proton signals at δ = 6.360 and 6.365 ppm (doublets, 1H each). The NH protons appear as singlets at δ = 11.048 ppm. The 2,4-dinitrobenzylidene group exhibits resonances at δ = 7.040, 7.215 and 9.522 ppm (doublets, 1H each), The $\mathbf{C^{13}}$ NMR spectrum shows pyrrole carbon resonances at 120.241 ppm (*C* = *C*) and 128.512 ppm (C—N), while the 2,4-dinitrobenzylidene carbons appear at 130.350, 131.502, 133.620, and 135.427 ppm (*C* = *C*), with the imine carbon detected at 186.299 ppm (C—N). An additional peak at 111.709 ppm corresponds to a C—*C* = *C* environment.

Matrix-assisted laser desorption/ionization time-of-flight (MALDI-TOF) mass spectrometry was utilized to confirm the molecular structure and composition of the synthesized copolymers. The analysis revealed an average molecular weight (Mn) of 1066.193 for PP3NB and 1199.563 for PPDNB, verifying that the successful synthesis was consistent with the intended molecular architectures. These detailed NMR and mass spectrometry results substantiate the formation of the designed copolymers, laying a robust foundation for further studies of their optoelectronic and morphological properties. Future research will explore their electronic behaviour, structural stability, and potential in advanced material systems.

4.2. Morphological properties

Scanning electron microscopy (SEM) analysis of dip-coated copolymer thin films revealed detailed surface morphologies, highlighting the strong link between molecular composition and microstructure [13]. PP3NB exhibited a remarkably smooth surface with minimal roughness, which is ideal for applications requiring efficient charge transport and reduced optical scattering. Conversely, PPDNB displayed a more intricate morphology with moderate roughness and a uniform distribution of nanoscale features, suggesting subtle molecular interactions during film formation. Both copolymers demonstrated consistent substrate coverage and dispersion, reflecting robust film-forming properties despite compositional differences. These morphological variations emphasize the pivotal role of molecular design in tailoring thin-film characteristics, with significant potential for electronic, photonic, and optoelectronic technologies. The differences likely stem from variations in molecular weight, solubility, and substituent effects, with PPDNB's higher molecular weight and solubility in dichloromethane contributing to its granular texture [14–16].

Fig. 3.

Cross-sectional SEM images (Fig. 4) showed that the copolymer thin films, with thicknesses of 35–38 nm, exhibited excellent continuity and strong adhesion to glass substrates, free of visible cracks or defects. The films' morphological traits smooth surfaces in PP3NB for uniform charge transport and low interfacial resistance and improving oxidation processes such as pollutant degradation or water oxidation, thanks to better charge separation [7], versus rougher surfaces in PPDNB for improved light scattering and greater surface area directly impact their optoelectronic feasibility which improves photon absorption and provides more sites for reduction reactions, such as hydrogen evolution or CO_2 reduction [8]. These morphological differences allow for performance optimization via substituent modification, with PP3NB being more suitable for oxidation and PPDNB for reduction, making them promising for tandem photocatalytic systems.

4.3. Optical properties

The optical properties of dip-coated copolymer thin films were examined using UV–Vis spectroscopy to assess their light absorption and bandgap energies. These are key factors in evaluating their suitability for optoelectronic and photocatalytic applications [17]. The absorption spectra (Fig. 5) revealed broad visible-region absorption, with distinct peaks from π-π* transitions in the conjugated polymer backbone. Maxima in the near-ultraviolet range (above 4 eV) indicated strong light-harvesting efficiency at higher energies. PP3NB and PPDNB exhibited similar profiles, with intense visible absorption tapering into the near-infrared. Optical bandgaps (Eg) were determined via Tauc plot analysis, based on the relation $(Ah\nu = A(h\nu - Eg)^n)$, where α is the absorption coefficient, hν is photon energy, A is a constant, and it reflects the transition type (direct or indirect). The resulting bandgaps—approximately 2.1 eV for PP3NB and 1.98 eV for PPDNB confirm their semiconductor nature and suitability for visible-light absorption, positioning them as promising materials for organic solar cells and photocatalysis.

The copolymer thin films' optical properties marked by broad visible-region absorption and bandgaps aligned with the solar spectrum highlight their potential for optoelectronic and photocatalytic applications. In organic solar cells, these traits enable efficient light harvesting and charge carrier generation. At the same time, their strong visible-light absorption and semiconductor characteristics suit them for photocatalytic processes like water splitting and pollutant degradation. The tunable absorption and bandgap energies, modulated by benzylidene substituents, emphasize the materials' versatility, allowing optimization for diverse renewable energy and environmental remediation applications.

4.4. Electrochemical properties

The electrochemical properties of the synthesized copolymers were evaluated using cyclic voltammetry (CV) to determine their oxidation and reduction potentials, enabling estimation of the highest occupied molecular orbital (HOMO) and lowest unoccupied molecular orbital (LUMO) energy levels—critical parameters for understanding charge

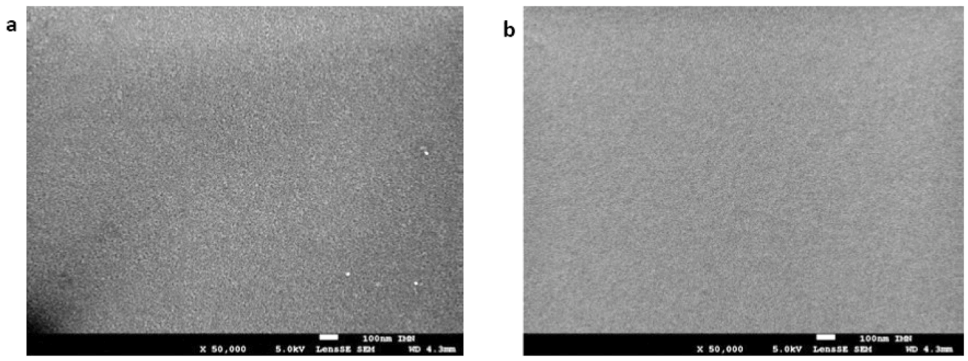

Fig. 3. SEM micrograph of the surface morphology of P: P–B dip-coated films for copolymers: (a) PP3NB, (b) PPDNB.

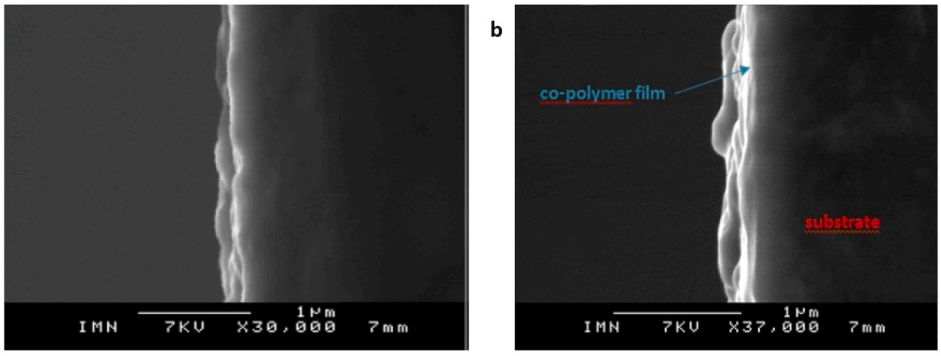

Fig. 4. Cross-sectional SEM images of P: P–B dip-coated films for copolymers: (a) PP3NB, (b) PPDNB.

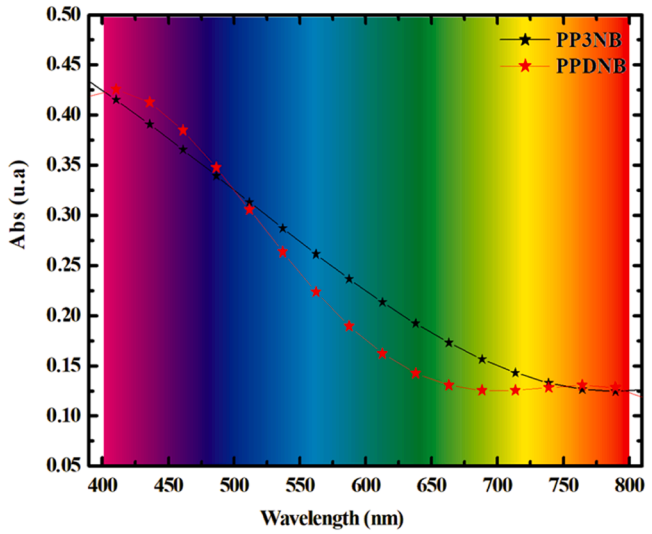

Fig. 5. Optical absorbance spectra in the visible region of PP3NB and PPDNB: thin films containing various benzylidene derivatives.

carrier generation and transport in optoelectronic devices. CV measurements were conducted in a 0.1 M tetrabutylammonium perchlorate (TBAP) electrolyte solution under a nitrogen atmosphere at room temperature, with a scan rate of 100 mV s^{-1}. The oxidation (E_p) and reduction (E_n) potentials were recorded, and the HOMO and LUMO levels were subsequently calculated using established equations [18–22].

$$E_{HOMO} = -(Ep + 4.4\ eV) \tag{8}$$

$$E_{LUMO} = -(En + 4.4\ eV) \tag{9}$$

The energy gap (*Eg*) was subsequently determined as the difference between the LUMO and HOMO energy levels:

$$Eg = E_{LUMO} - E_{HOMO} \tag{10}$$

This approach provided a reliable method for evaluating the copolymers' electrochemical properties, enabling the correlation of their electronic structure with their optoelectronic and photocatalytic feasibility. Cyclic voltammetry (CV) curves (Fig. 6) displayed distinct oxidation and reduction peaks for each copolymer, allowing calculation of their HOMO and LUMO energy levels: for PP3NB, *E*HOMO=−6.1 eV and LUMO=−3.9 eV; for PPDNB, *E*HOMO=−6.08 eV and *E*LUMO=−4.09 eV. The resulting bandgaps, ranging from 1.9 to 2.2 eV, closely matched optical bandgap values from UV–Vis spectroscopy, confirming measurement reliability and validating the copolymers' electronic properties.

4.5. The significance of effective mass in photocatalysis

The effective mass (m*) of charge carriers is a key factor in determining the photocatalytic efficiency of semiconductor materials. In photocatalysis, the mobility and separation of photogenerated electrons and holes critically influence charge transfer dynamics and overall feasibility. A lower m* enhances carrier mobility, reducing recombination rates and improving charge transport to reactive sites properties vital for applications like water splitting, CO_2 reduction, and pollutant degradation [23,24]. We calculated their effective masses to assess the charge transport capabilities of PP3NB and PPDNB, offering insights into their photocatalytic potential. Materials with optimized m* exhibit enhanced light absorption and charge utilization, making control of this parameter essential for designing high- feasibility photocatalysts. For organic semiconductors and conjugated polymers, where traditional band structure calculations are challenging, m* can be approximated using HOMO and LUMO energy levels. In these systems, the conduction and valence bands are represented by the lowest unoccupied molecular

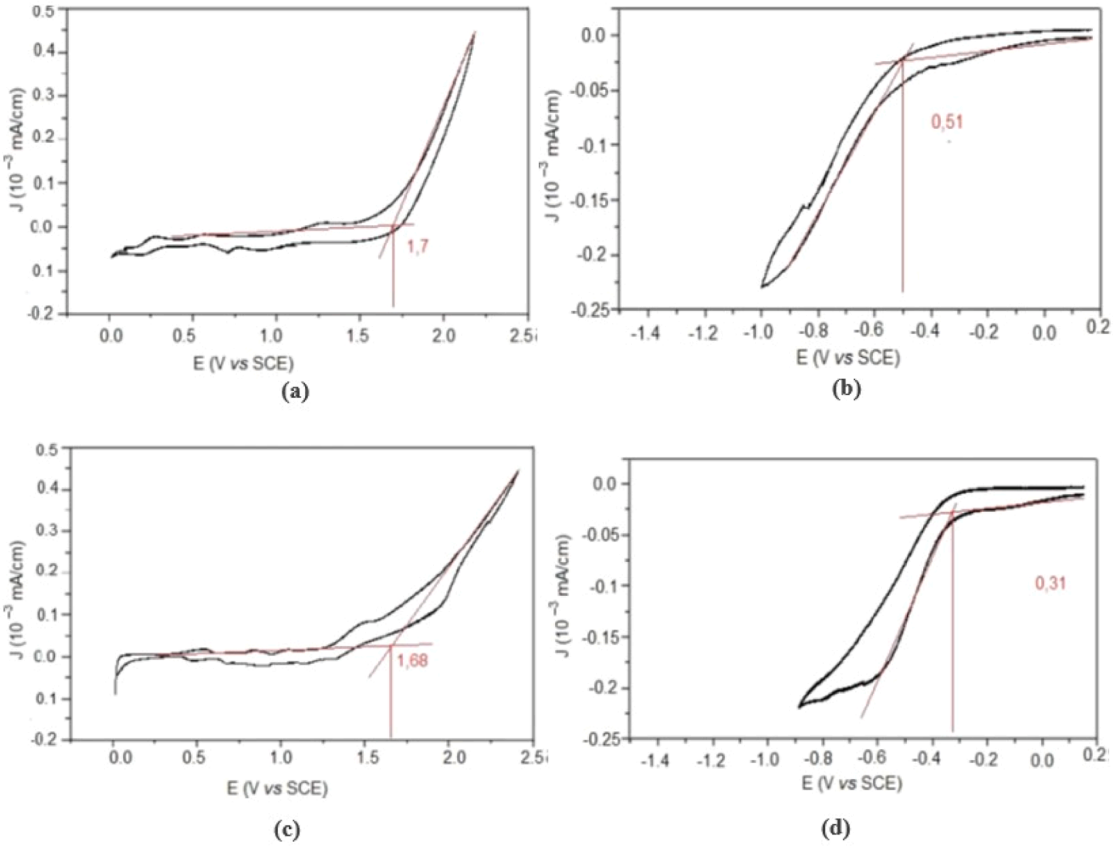

Fig. 6. Cyclic voltammetry curves showing oxidation and reduction, respectively of PP3NB (a, b), PPDNB (c, d) in CH_2Cl_2.

orbital (LUMO) and highest occupied molecular orbital (HOMO), respectively. A simplified estimation of m* is derived from the relation provided [25,26].

$$m^* \approx \frac{\hbar^2}{2}\left(\frac{d^2E}{dk^2}\right)^{-1} \tag{11}$$

E is the energy, k is the wavevector, and $\hbar$ is the reduced Planck's constant. Since $\frac{d^2E}{dk^2}$ is related to the curvature of the band, we approximate it using the energy difference between HOMO and LUMO:

$$m^* \approx \frac{\hbar^2}{2E_gL^2} \tag{12}$$

where: $E_g = E_{LUMO} - E_{HOMO}$,

L = characteristic molecular length or conjugation length (nm).

The conjugation length (L) denotes the extent of π-electron delocalization in a conjugated polymer, directly affecting its electronic properties, such as bandgap (Eg) and charge transport. Literature suggests π-conjugation lengths typically span 1.5–3.0 nm, with shorter lengths (~1.5 nm) linked to structural defects or steric hindrance, and longer lengths (~3.0 nm) observed in well-ordered, extended π-systems [27]. Given our polymers' moderate bandgaps (~2.0 eV), an estimated L of approximately 1.5 nm is deemed suitable for characterizing their electronic structure and charge transport behavior. To determine the conjugation length more precisely, we applied the exciton Bohr radius approach using the absorption onset wavelength (λ_{onset}) from UV–Vis spectra. The conjugation length is estimated using the relation:

$$L \approx \frac{hc}{E_g} \tag{13}$$

where: h = Planck's constant (6.626×10^{-34} J·s), c = speed of light (3.0×10^8m/s), Eg = band gap in Joules. Using this approach, we calculated conjugation lengths of 1.64 nm for PP3NB and 1.78 nm for PPDNB, reflecting significant π-electron delocalization in their structures. These values determined the effective masses of charge carriers as 0.00635 m_e for PP3NB and 0.00596 m_e for PPDNB. These low values underscore the polymers' excellent charge transport properties, enhancing their suitability for optoelectronic and photocatalytic applications requiring high charge mobility.

4.6. Photocatalytic suitability of PP3NB and PPDNB

The photocatalytic activity of a material depends heavily on the alignment of its valence band (E_{VB}) and conduction band (E_{CB}) with the redox potentials of target reactions. This study assessed the band edge positions of the conjugated copolymers PP3NB and PPDNB relative to the normal hydrogen electrode (NHE) scale. PP3NB exhibited E_{VB}=+1.6 V and E_{CB}=−0.6 V, while PPDNB showed E_{VB}=+1.58 V and E_{CB}=−0.41 V. These values indicate distinct oxidation and reduction capacities, shaping their suitability for various photocatalytic applications. For efficient oxidation reactions, such as water oxidation (O_2/H_2O) or organic pollutant degradation, a photocatalyst's valence band (E_{VB}) must exceed the reaction's redox potential. With water oxidation at +1.23 V (NHE), both PP3NB (+1.6 V) and PPDNB (+1.58 V) meet this requirement (Fig. 7). However, PP3NB's higher E_{VB} confers greater oxidative strength, enhancing its feasibility in generating potent species like hydroxyl radicals (**$OH^{\bullet}$**) for advanced oxidation processes. This suggests PP3NB's superior potential for environmental remediation, including pollutant degradation and organic dye removal.

$$H_2O \rightarrow O_2 + 4H^+ + 4e^- \quad (E^0 = +1.23\ V\ NHE) \tag{14}$$

On the other hand, a photocatalyst's ability to drive reduction

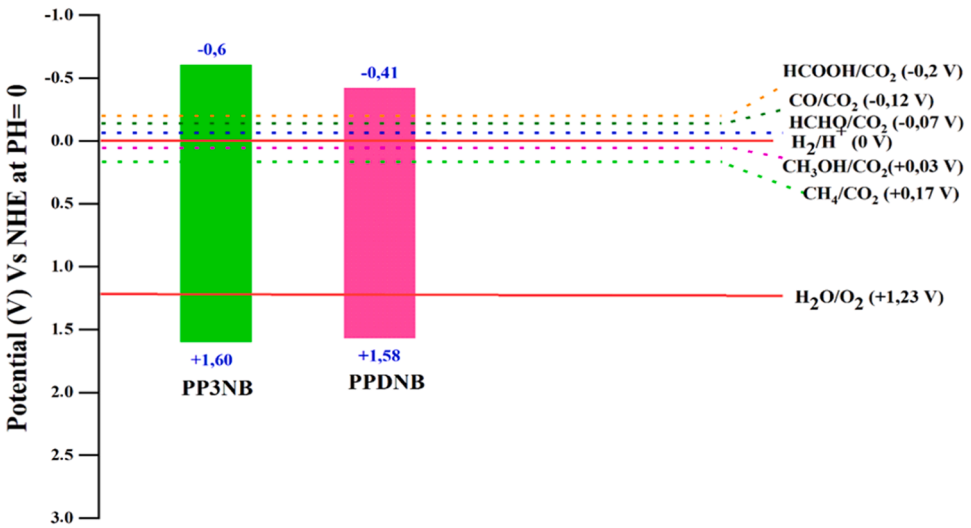

Fig. 7. Band edges of PP3NB and PPDNB to the redox potentials of the water-splitting reaction and CO_2 reduction photodegradation processes at standard hydrogen electrode (NHE) scale at pH = 0.

reactions, such as hydrogen evolution (H_2 production) or oxygen reduction, hinges on its conduction band (E_{CB}) being sufficiently negative relative to the target redox potential. Hydrogen evolution requires an E_{CB} below 0.00 V (NHE), while superoxide formation ($O_2^{\bullet-}$) demands a value under −0.33 V (NHE). Both PP3NB (−0.6 V) and PPDNB (−0.41 V) satisfy these criteria for proton reduction to H_2 and oxygen reduction to ($O_2^{\bullet-}$). However, PP3NB's more negative E_{CB} suggests greater efficiency in reduction-driven photocatalysis, favoring its use in hydrogen evolution applications.

$$2H^+ + 2e^- \rightarrow H_2 \ \left(E^0 = 0.00\ V\ NHE \right) \quad (15)$$

The complementary attributes of PP3NB and PPDNB suggest their potential in tandem photocatalytic systems, with PP3NB driving oxidation processes and PPDNB facilitating reduction reactions. This pairing could improve charge separation efficiency and expand the scope of photocatalytic applications. However, despite their favorable band structures, factors such as charge carrier dynamics, interfacial recombination, photostability, and durability require further investigation to confirm their suitability for large-scale use. Future research should optimize these materials through heterojunctions, co-catalysts, and surface engineering to boost photocatalytic feasibility.

The comparative discussion positions PP3NB and PPDNB against common photocatalysts, including metal oxides (TiO_2, ZnO), MOFs (UiO-66, ZIF-8), and other conjugated polymers (P3HT, polypyrrole). TiO_2 and ZnO, while stable, are limited to UV absorption, requiring complex modifications for visible activity. MOFs offer high porosity and surface area, but their visible absorption and stability pose challenges, often addressed by hybridization [28]. P3HT and polypyrrole absorb in the visible region but suffer from rapid charge recombination and limited stability [29]. In comparison, PP3NB and PPDNB absorb efficiently in the visible region, with band potentials suitable for complementary redox reactions. Their tunable morphologies (smooth for PP3NB, granular for PPDNB) optimize charge transport and active surface area, potentially outperforming oxides and conjugated polymers in terms of photocatalytic efficiency, while offering simpler organic synthesis than MOFs. These characteristics position them as promising alternatives for water splitting and CO_2 reduction.

5. Conclusion

The newly synthesized materials display broad absorption in the visible spectrum, low effective mass, and well-aligned HOMO–LUMO energy levels, which collectively promote efficient charge transport and separation. Morphological analysis revealed the formation of high-quality thin films with tunable surface roughness, influencing both light harvesting and interfacial charge dynamics. Electrochemical measurements further confirmed their semiconducting character, with HOMO–LUMO levels ideally positioned for photocatalytic applications. Photocatalytic evaluation revealed the highest reduction capacity of PPDNB promotes hydrogen production and CO_2 reduction, while PP3NB has the feasibility as an oxidation catalyst, ideal for pollutant degradation and oxygen release. Their complementary characteristics suggest a suitability for tandem photocatalytic systems, optimizing charge separation and redox feasibility. These results position PP3NB and PPDNB copolymers as promising next-generation materials, bridging organic semiconductors with advanced functional technologies such as optoelectronic and photocatalytic applications.

CRediT authorship contribution statement

Abderrahmane Remil: Conceptualization. **Mohamed El Amine El Goutni:** Data curation. **Talal M. Althagafi:** Data curation. **Mokhtar Saidi:** Conceptualization. **Hamza Belkhodja:** Formal analysis. **Abdelkrim Bendoukha Reguig:** Data curation. **Mohammed El Amine Monir:** Data curation. **M. Fatmi:** Validation. **M.A. Ghebouli:** Formal analysis.

Declaration of competing interest

The authors declared no potential conflicts of interest with respect to the research, authorship, and/or publication of this article.

Acknowledgements

The authors extend their appreciation to Taif University, Saudi Arabia, for supporting this work through project number (TU-DSPP-2024-208).

Data availability

No data was used for the research described in the article.

References

[1] B. Mortazavi, M.E. Madjet, M. Shahrokhi, S. Ahzi, X. Zhuang, T. Rabczuk, Carbon nanostructures for multifunctional applications, Carbon N Y 147 (2019) 377–389, https://doi.org/10.1016/j.carbon.2019.03.010.

[2] J. Yu, D. Sun, T. Wang, F. Li, Enhanced catalytic activity of nanostructured materials for environmental remediation, Chem. Eng. J. 334 (2018) 225–234, https://doi.org/10.1016/j.cej.2017.10.086.
[3] K.R. Reddy, M. Hassan, V.G. Gomes, Nanostructured catalysts for sustainable energy, Appl. Catal. A Gen. 489 (2015) 1–12, https://doi.org/10.1016/j.apcata.2014.10.021.
[4] A. Roy, H.C.P. Movva, B. Satpati, K. Kim, R. Dey, A. Rai, T. Pramanik, S. Guchhait, E. Tutuc, S.K. Banerjee, Hybrid nanomaterials for multifunctional devices, ACS Appl. Mater. Interfaces 8 (2016) 7396–7402, https://doi.org/10.1021/acsami.6b00961.
[5] D. Pla, C. Jimenez, M. Burriel, Interface engineering for improved material performance, Adv. Mater. Interfaces 4 (2017) 1600974, https://doi.org/10.1002/admi.201600974.
[6] X. Mu, F. Yang, Q. Guo, Y. Zhang, Y. Chen, T. Jiang, Bimetallic synergy in Si-$(CH_2)_n$-Si-bridged binuclear indenyl-pyrrolidinyl titanium catalysts for ethylene/1-octene copolymerization, Mol. Catal. 581 (2025) 115145, https://doi.org/10.1016/j.mcat.2025.115145.
[7] L. Chen, L. Gao, X. Zhang, X. Liu, Q. Chen, J. Li, Y. Zhang, T. Liu, Nickel phthalocyanine based porous bimetallic catalysts for high activity CO_2 electroreduction over wide potential window, Mol. Catal. 581 (2025) 115039, https://doi.org/10.1016/j.mcat.2025.115039.
[8] B. Wang, R. Gao, X. Geng, J. Wang, L. Wang, H. Chen, B. Zhu, Photocatalyzed C3-α-aminoalkylation of quinoxalin-2(1H)-ones with amino acid-derived oxime esters under metal-free conditions, Mol. Catal. 573 (2025) 114795, https://doi.org/10.1016/j.mcat.2024.114795.
[9] A. Remil, Y. Mouchaal, A.B. Reguig, A.L. Toumi, H. Gherrass, A. Hachemaoui, A. Yahiaoui, A. Khelil, Synthesis of new nitrobenzylidene derivatives and pyrrole-based copolymers for dye-sensitized solar cells: effect of substituent on opto-electrical properties of dip-coated thin films, Surf. Rev. Lett. 25 (2018) 1850116, https://doi.org/10.1142/S0218625X18501160.
[10] A.O. Ibhadon, P. Fitzpatrick, Heterogeneous photocatalysis: recent advances and applications, Catalysts 3 (2013) 18–50, https://doi.org/10.3390/catal3010018.
[11] R. Beranek, Advances in physical chemistry of nanomaterials, Adv. Phys. Chem. 2011 (2011) 786759, https://doi.org/10.1155/2011/786759.
[12] H. Yan, X. Wang, M. Yao, X. Yao, Photocatalytic materials: progress and challenges, Prog. Nat. Sci. Mater. Int. 23 (2013) 402–407, https://doi.org/10.1016/j.pnsc.2013.06.004.
[13] Y. Chen, Y. Park, I. Noda, Y.M. Jung, Molecular structure analysis via spectroscopy, J. Mol. Struct. 1124 (2016) 159–166, https://doi.org/10.1016/j.molstruc.2016.06.033.
[14] M. Nakashima, R. Kikuchi, K. Omura, Y. Suda, T. Sato, A. Mori, S. Hayase, L. Han, Disilanobithiophene–dithienylbenzothiadiazole alternating polymer as donor material of bulk heterojunction polymer solar cells, Polym. J. 47 (2015) 404–410, https://doi.org/10.1038/pj.2015.61.
[15] S. Lu, K. Liu, D. Chi, S. Yue, Y. Li, K. Yanlei, X. Lin, Z. Wang, S. Qu, Z. Wang, Constructing bulk heterojunction with componential gradient for enhancing the efficiency of polymer solar cells, J. Power Sources 300 (2015) 238–244, https://doi.org/10.1016/j.jpowsour.2015.09.079.
[16] J.U. Lee, J.W. Jung, T. Emrick, T.P. Russell, W.H. Jo, Nanostructured polymer blends for electronics, Nanotechnology 21 (2010) 105201, https://doi.org/10.1088/0957-4484/21/10/105201.
[17] A.L. Toumi, A. Khelil, J.C. Bernède, Y. Mouchaal, A. Djafri, K. Toubal, N. Hellal, L. Cattin, Optimum compromise between optical absorption and electrical property of the planar multi-heterojunction organic solar cells based with new thiazol derivative, the (2-thioxo-3-n-(2-methoxyphenyl) thiazolidin-4-one), as electron donor, Surf. Rev. Lett. 22 (2015) 1550025, https://doi.org/10.1142/S0218625X15500250.
[18] D.M. de Leeuw, M.M.J. Simenon, A.R. Brown, R.E.F. Einerhand, Organic semiconductors: synthesis and applications, Synth. Met. 87 (1997) 53–59, https://doi.org/10.1016/S0379-6779(97)80001-4.
[19] J. Qin, H. Wu, Y. Dong, F. Zhan, M. Liao, B. Pan, C. Wang, Polymerization synthesis of semi-coke activated carbon modified carbon nitride nanoscrolls with boosted photocatalytic H_2 production, Mol. Catal. 556 (2024) 113918, https://doi.org/10.1016/j.mcat.2024.113918.
[20] G. Kim, Y.E. Kim, J. Jae, M.S. Lee, Effect of physicochemical properties of carbons on the performance of bead-type Pd/C catalysts for furfural hydrogenation, Mol. Catal. 558 (2024) 114025, https://doi.org/10.1016/j.mcat.2024.114025.
[21] Y. Zhao, J. Sun, H. Xu, Electrochromic properties of pyrene conductive polymers modified by chemical polymerization, Int. J. Mol. Sci. 23 (2022) 9044, https://doi.org/10.3390/ijms23159044.
[22] K. Qu, M. Fang, S. Zhang, H. Liu, X. Zeng, A redox conjugated polymer-based all-solid-state reference electrode, Polymers 10 (2024) 1191, https://doi.org/10.3390/polym10111191.
[23] S. Jiang, Q. Zhang, W. Li, J. Peng, Y. Zhou, G. He, Electrocatalytic oxidation of methane to low-carbon alcohol via stable Ni^{+}/ni^{0} interface, Mol. Catal. 563 (2024) 114234, https://doi.org/10.1016/j.mcat.2024.114234.
[24] Y. Cao, S. Alsharif, A.S. El-Shafay, Novel semiconductor materials, Mater. Sci. Semicond. Process. 144 (2022) 106569, https://doi.org/10.1016/j.mssp.2022.106569.
[25] M. Heydari Gharahcheshmeh, K.K. Gleason, Advanced materials for electronics, Mater. Today Adv. 8 (2020) 100086, https://doi.org/10.1016/j.mtadv.2020.100086.
[26] M. Wang, Y. Zhang, H. Li, Density functional theory calculations unveil strongly dispersive energy bands with small electron–hole reduced effective masses (~0.15 m_0) for two-dimensional conjugated polymers, J. Mater. Chem. C 11 (2023) 10335–10342, https://doi.org/10.1039/d3tc01234a.
[27] J. Rissler, Molecular simulations in chemistry, Chem. Phys. Lett. 395 (2004) 92–97, https://doi.org/10.1016/j.cplett.2004.07.024.
[28] Z. Li, J. Liang, W. Fan, Bi-functional S-scheme Bi2WO6/NiO heterojunction for photocatalytic ciprofloxacin degradation and CO_2 reduction: mechanisms and pathways, Sep. Purif. Technol. 310 (2023) 123197, https://doi.org/10.1016/j.seppur.2023.123197.
[29] Y. Li, D. Huang, Z. Yu, Bi2WO6/TiO2/Ti3C2 S-scheme heterojunction for enhanced photocatalytic performance, Inorg. Chem. Commun. 143 (2022) 109826, https://doi.org/10.1016/j.inoche.2022.109826.